Mapping thalamic-anterior cingulate monosynaptic inputs in adult mice

Man Xue[1], Wan-Tong Shi[1], Si-Bo Zhou[1], Ya-Nan Li[2], Feng-Yi Wu[3], Qi-Yu Chen[2,3] (iD),
Ren-Hao Liu[1], Zhao-Xiang Zhou[1], Yu-Xiang Zhang[2], Yu-Xin Chen[1], Fang Xu[3],
Guo-Qiang Bi[3], Xu-Hui Li[1,2] (iD), Jing-Shan Lu[1,2] (iD), and Min Zhuo[1,2,4]

Abstract

The anterior cingulate cortex (ACC) is located in the frontal part of the cingulate cortex, and plays important roles in pain perception and emotion. The thalamocortical pathway is the major sensory input to the ACC. Previous studies have show that several different thalamic nuclei receive projection fibers from spinothalamic tract, that in turn send efferents to the ACC by using neural tracers and optical imaging methods. Most of these studies were performed in monkeys, cats, and rats, few studies were reported systematically in adult mice. Adult mice, especially genetically modified mice, have provided molecular and synaptic mechanisms for cortical plasticity and modulation in the ACC. In the present study, we utilized rabies virus-based retrograde tracing system to map thalamic-anterior cingulate monosynaptic inputs in adult mice. We also combined with a new high-throughput VISoR imaging technique to generate a three-dimensional whole-brain reconstruction, especially the thalamus. We found that cortical neurons in the ACC received direct projections from different sub-nuclei in the thalamus, including the anterior, ventral, medial, lateral, midline, and intralaminar thalamic nuclei. These findings provide key anatomic evidences for the connection between the thalamus and ACC.

Keywords

Thalamus, anterior cingulate cortex, mapping, volumetric imaging with synchronized on-the-fly-scan and readout, retrograde projection

Date Received: 22 December 2021; Revised 8 February 2022; accepted: 22 February 2022

Introduction

The thalamus is located in the middle of the brain, and can be anatomically subdivided into several major nuclear regions, including the anterior, ventral, medial, lateral, midline, intralaminar, medial and lateral geniculate body nuclei.[1,2] Different thalamic nuclei interconnect reciprocally with cerebral cortices.[2,3] Multiple cortical areas receive monosynaptic inputs from the thalamus. The thalamocortical pathways are essential for many key physiological functions, including sensory perception, motor coordination, and emotion.[4]

As a key cortical region, the anterior cingulate cortex (ACC) receives most inputs from different thalamic nuclei, which plays important roles in pain perception and emotional regulation.[5–7] Electrophysiological experiments using *in-vivo* thalamic stimulation in rats have confirmed the existence of thalamic-anterior cingulate projections. Electrical stimulation of mediodorsal (MD),

[1]Center for Neuron and Disease, Frontier Institutes of Science and Technology, Xi'an Jiaotong University, Xi'an, China
[2]Institute of Brain Research, Qingdao International Academician Park, Qingdao, Shandong 266199, China
[3]CAS Key Laboratory of Brain Connectome and Manipulation, Interdisciplinary Center for Brain Information, The Brain Cognition and Brain Disease Institute, Shenzhen Institute of Advanced Technology, Chinese Academy of Sciences; Shenzhen-Hong Kong Institute of Brain Science-Shenzhen Fundamental Research Institutions, Shenzhen, China
[4]Department of Physiology, Faculty of Medicine, University of Toronto, Toronto, ON, Canada

Corresponding Authors:
Jing-Shan Lu, Center for Neuron and Disease, Frontier Institutes of Science and Technology, Xi'an Jiaotong University, Xi'an 710049, China.
Email: lujs33@mail.xjtu.edu.cn

Min Zhuo, Institute of Brain Research, Qingdao International Academician Park, Qingdao, Shandong, China.
Email: min.zhuo@utoronto.ca

midline, and intralaminar thalamic nuclei induced short-term plastic changes in layers II/III of the ACC that transmit nociceptive information to the ACC in early stage of chronic pain.[8,9] In recent decades, most systematic anatomic studies based on neural tracers showed that major thalamic nuclei, such as anterior, ventral, medial, lateral thalamic nuclei, etc., send direct projections to the ACC in different species. For example, rhodamine and diamidino yellow were injected into the caudal/rostral area 24b of the ACC in the rabbit, respectively, to observe thalamic-anterior cingulate inputs, and find that the rostral area 24b receive a large proportion of projection fibers from the anteromedial (AM), ventroanterior (VA), mediodorsal (MD), and submedial (Sub) thalamic nuclei. However, the caudal area 24b injection produced heavy neuronal labeling in the AM, VA, ventrolateral (VL), and MD thalamic nuclei.[10] In addition, most anatomic studies about thalamic-anterior cingulate inputs have also been reported in monkeys,[11,12] rats,[13–15] and cats.[16,17] In recent decades, many studies have revealed molecular and synaptic mechanisms for cortical plasticity and modulation in the ACC of adult mice.[5-7] Recently, Clémentine Fillinger et al.[18] utilized the FluroGold (FG)/β-subunit of choleric toxin (CTb) dyes to trace afferents to the ACC rostral area 24a/b of mice, and found the area 24a and 24b receive some projection fibers from different thalamic nuclei, respectively; Oh et al.[3] also observed some thalamic-anterior cingulate projections by injecting green fluorescent protein (EGFP)-expressing adeno-associated viral vectors to trace anterogradely. Despite these reports using the dyes and anterograde viral tracing methods, more systematic anatomic studies are still needed in adult mice.

Here, we mainly utilized rabies virus-based monosynaptic retrograde tracing system, an effective method to map afferent presynaptic partners of the ACC in adult mice. Simultaneously, we combined a new microscopy method of Volumetric Imaging with Synchronized on-the-fly-scan and Readout (VISoR) for a three-dimensional (3D) brain reconstruction, which can achieve a high-speed, high-throughput, and high-quality brain mapping.[19,20] We found that cortical neurons in the ACC receive direct afferents from these thalamic nuclei, such as the AM, the ventromedial (VM), the anterior-lateral complex of the ventral (VAL), the centrolateral (CL), the lateral part of the mediodorsal (MDl), the mediorostral part of the lateral posterior (LPMR), the dorsomedial part of the laterodorsal (LDDM), the posterior (Po), the parafascicular (PaF), the ventrolateral part of the laterodorsal (LDVL), the interanteromedial (IAM), the angular (Ang), the Sub, the anterodorsal (AD), and other thalamic nuclei that have sparse projections to the ACC. These findings provide a basis for further investigation of thalamocortical circuitry mechanisms and functions.

Methods

Animals

Adult male C57BL/6 mice (aged 6–8 weeks) were purchased from Experimental Animal Center of Xi'an Jiaotong University.

Experimental animals were randomly housed in plastic cages with ad libitum access to enough food and water under a 12-h day/night cycle at the temperature of 22–25°C. Mice were raised under experimental environment at least 1 week before carrying out experiments. All experimental procedures were in accordance with the guidelines of the Ethics Committee of Xi'an Jiaotong University.

Viruses and surgery

All the viruses used in the trans-synaptic retrograde tracing experiments included rAAV-hSyn-EGFP-2a-TVA-2a-RVG-WPREs-pA (AAV2/9, 2.0 x 10^{12} genomics copies per mL) and EnvA-pseudotyped, glycoprotein (RG)-deleted and DsRed-expressing rabies virus (RV-EnvA-ΔG-DsRed, RV; 2.0×10^8 genomic copies per mL) were bought from Brainvta company (Wuhan, China). Viral injection was performed as previously described.[21] Briefly, the experimental mice were anesthetized under 2% isoflurane and fixed on a stereotaxic apparatus to adjust the skulls in order to be parallel to the reference panel. The skull was drilled a hole on the right side of the ACC (0.90 mm anterior to the bregma, 0.30 mm lateral to the midline, 1.40 mm ventral to the surface of the skull). Using a microsyringe pump (Nanoject II #3-000-205/206, DRUMMOND), AAV viruses with a volume of 200 nL were first stereotaxically injected (23 nL/min, once every 10 seconds) into the right side of the ACC with equal speed. Next, an additional 10 min was kept to allow diffusion of viral particles away from the injection site before the glass electrode was slowly withdrawn. After 21-day expression of helper viruses, 200 nL of RV-EnvA-ΔG-DsRed was injected into the same location and was expressed for 7 days.[22]

Brain slice seperation and imaging

After 7 days of RV virus expression, the experimental mice were anaesthetized and perfused with 0.01 M phosphate buffered saline (PBS) followed by 4% paraformaldehyde (PFA) in PBS (pH 7.4). The whole brain was separated and stored in 4% PFA solution for 4-hour post-fixation. And then, the whole brain was transferred into 30% sucrose solution (m/v) for 3-day dehydration. 30 μm-thick coronal brain slices were prepared using a cryostat (Leica CM1900). Every third section was mounted onto the slides and counterstained with DAPI (SB0027, Bio-fount), and then visualized with an Olympus VS200 microscope (20x objective).

To acquire one 3D-reconstructed whole brain, we used a high-speed and high-throughput VISoR imaging to reconstruct series of 2D images from 300 μm-thick coronal brain slices as previously described.[19,20] The separated whole brain in 4% PFA solution was transferred into 4% acrylamide hydrogel monomer solution (HMS) in PBS (w/v) for 2 days at 4°C. Next, the whole brain was fixed and cut into 300 μm-thick coronal brain slices (40-50 slices for one mouse). These slices were transferred into clearing solution (5% PBS-Triton) for 24 h at 37°C. After washing out for three times with PBS, these slices were mounted onto the quartz slides in sequence

Table 1. Summary of previous studies on thalamic-anterior cingulate projections.

Species	Thalamic nuclei						References
	Anterior	Lateral	Ventral	Medial	Midline	Intralaminar	
Rats	++	++	++	+++	+++	+++	13-15, 23, 43–45
Monkeys	++	+	++	++	++	++	11, 12, 46, 47
Cats	++	+	++	+	++	++	16, 17, 48
Mice	++	++	++	++	++	++	3, 18, 22, 25, 49
Rabbits	+	+	+	+	+	+	10

*+++: more than 5 references reported; ++: 3–5 references reported; +: less than 3 references reported.

and were fixed with 4% HMS at 37°C for 4 h. The slide with fixed slices was immersed into refractive-index-matching solution. The slices were visualized with synchronized beam-scan illumination and camera-frame readout (10x objective). The resultant voxel size is 0.5x0.5x3.5 μm^3.

Statistical analysis

We divided the thalamic nuclei according to the Mouse Brain in Stereotaxic Coordinates, 4th edition. The cell densities and the number of neurons were analyzed by Olympus analysis software and Image J software. The most labeled unit area was chosen for cell density analysis in every brain region. All data was presented as mean ± SEM and the histogram was plotted with OriginPro 8.0 software. Two-tail unpaired *t*-test were used for statistical comparisons. In all cases, $p < 0.05$ was considered to be the criterion for statistical significance.

Results

### Summary of previous studies on thalamic-anterior cingulate projections

In past several years, studies have reported anatomic connections and functional characteristics between different thalamic nuclei and the ACC. Here, we summarized previous reports about afferents to the ACC from thalamic nuclei in different species (Table 1). The update of different tracing strategies that contains anterograde, retrograde tracers, and viral tracing strategies, gives us a deeper understanding of whole-brain anatomic connections. We found that these projected neurons to the ACC mainly focus on the AM of the anterior group, the VAL and VM of the ventral group, the laterodorsal thalamic nucleus (LD), and lateral posterior thalamic nucleus (LP) of the lateral group, MD thalamic nucleus of the medial group, the central medial thalamic nucleus (CM), paracentral thalamic nucleus (PC), CL, PaF, and rhomboid thalamic nucleus (RH) of the intralaminar group and the reuniens thalamic nucleus (RE) of the midline nuclei. Studies have also shown that cortical projections of thalamic nuclei are predominantly ipsilateral, except for the midline nuclei. A small number of thalamocortical neurons in

the midline group send projections to the contralateral cortices.[18,23]

VISoR imaging to observe presynaptic afferents to the ACC

In recent years, large-scale 3D imaging has become an increasingly important approach in the study of the brain circuitry mechanisms and functions. The VISoR systems can achieve a fast 3D image acquisition followed with synchronized scanning beam illumination and oblique imaging over cleared tissue sections.[19,20] Here, we utilized VISoR imaging combined with rabies virus-based monosynaptic retrograde tracing system for a 3D whole-brain reconstruction to observe presynaptic monosynaptic inputs to the ACC in adult mice. On the first day, the helper virus was stereotaxically micro-injected into the right side of ACC in adult mice (rAAV-hSyn-EGFP-2a-TVA-2a-RVG-WPREs-pA). On the role of the promoter hSyn, the EGFP, TVA, and RVG proteins were all expressed in ACC neurons. After 21 days, the rabies virus (RV-EnvA-ΔG-DsRed) was also stereotaxically micro-injected into the same location, which can infect mammalian cells with the cognition of cognate receptor TVA and an avian virus envelope protein (EnvA) (Figure 1(a) and (b)). With the help of RVG proteins from helper virus, the rabies virus then retrogradely spread to the upstream cells. Because of the absence of RVG proteins in the upstream cells, the trans-synaptic infection of the rabies virus is stopped. This strategy achieves trans-monosynaptic and retrograde spread. Seven days after the last injection, mice were perfused with 0.01 M PBS followed by 4% PFA in PBS (pH 7.4). 300 μm-thickness coronal brain slices were prepared for VISoR imaging.

3D reconstruction of the whole brain (Figure 2(a)) was performed according to the volumetric imaging data. More clearly and stereoscopically, the horizontal, sagittal, and coronal views of the whole brain were displayed in Figure 2(b)–(d). In the injection site of ACC, the cells only infected by rAAV were EGFP$^+$ (Figures 1(c)–(d), 2(a)–(d); green). Those neurons in the ACC called starter neurons which were both infected by rAAV (EGFP$^+$) and RV (DsRed$^+$) (Figures 1(c)–(d), 2(a)–(d); yellow). The
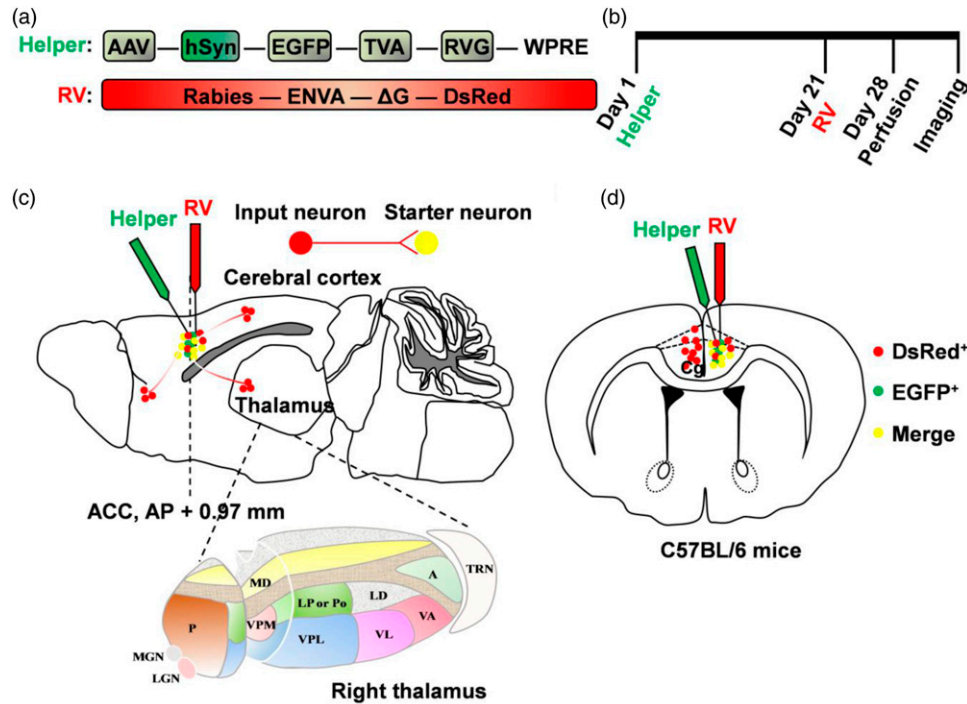
Figure 1. Schematic diagrams of afferents to the ACC neurons using rabies virus-based trans-monosynaptic tracing strategy. **(a)** The AAV helper virus with TVA receptor, RVG and EGFP; and the glycoprotein (G)-deleted rabies virus with EnVA and DsRed. **(b)** Experimental timeline of two viral injections. **(c–d)** Schematic diagrams of sagittal **(c)** and coronal **(d)** sections for showing the combination of two viruses micro-injected into the ACC and brain-wide labeling of monosynaptic inputs, especially the thalamus. The bottom figure in **(c)** indicates the enlarged schema of right thalamus. The green dots represent the neurons labeled by helper virus; the red dots represent the neurons sending presynaptic inputs to the ACC; the yellow dots represent the starter neurons, which are infected by both the helper virus and the rabies virus, and receive presynaptic inputs.

neurons which only showed DsRed$^+$ represented presynaptic inputs to starter neurons (Figures 1(c)–(d), 2(a)–(g); red). We found that the ACC received direct presynaptic inputs from different cerebral cortices, non-cortical forebrain areas, diencephalon, brainstem and so on.

Here, we mainly focused on the direct thalamic-anterior cingulate monosynaptic inputs. The three-dimensional views of the thalamus were displayed in Figure 2(e)–(g), and the input neurons and the projected fibers were apparent. We also displayed the horizontal, sagittal, and coronal sections which contained the AM, MD, and VM of the thalamus, respectively, which have heavy neuronal labeling (Figure 3(a)–(c), the intersection of two white lines represents thalamic nucleus). Overall, the VISoR system provides a high-efficiency and advanced approach for further study of brain mapping, which helps us to explore the systematisms of the brain and is beneficial for the treatment of brain-related diseases.

The in-situ viral expression for rabies-based retrograde tracing system in the ACC

For the past decades, more advanced studies and anatomic evidences made us better understand the mechanism of brain circuits. However, the dyes and the anterograde viral tracing have certain limits based on the study of afferents to the ACC, therefore, the rabies virus-based retrograde tracing strategy provides an effective method for tracing whole-brain afferents to the ACC. Here, we provided a detailed analysis about in-situ viral expression in the ACC. The separated brain was cut into 30 μm-thick coronal brain slices for VS200, confocal imaging, and further analysis. In the injection site of ACC, we observed EGFP$^+$, DsRed$^+$, and starter neurons from four representative coronal slices (Figure 4(a)–(c)). A total of twelve slices from four mice were chosen for statistical analysis of cell density at different coronal sections of the ACC separately. Firstly, we analyzed the cell density of EGFP$^+$ neurons and found that these neurons were highly expressed at AP +0.85 mm (Figure 4(d); cell densities: 464.07 ± 48.49 cells/mm^2 at AP +1.21 mm; 722.51 ± 34.07 cells/mm^2 at AP +0.85 mm; 600.78 ± 55.61 cells/mm^2 at AP +0.25 mm; **$p < 0.01$ for AP +1.21 mm versus +0.85 mm; unpaired t-test; $n = 12$ slices/4 mice). Secondly, more starter neurons were also observed at AP +0.85 mm (Figure 4(b) and (d); cell densities: 107.84 ± 22.21 cells/mm^2 at AP +1.21 mm; 246.40 ± 18.22 cells/mm^2 at AP +0.85 mm; 134.10 ± 13.49 cells/mm^2 at AP +0.25 mm; **$p < 0.01$ for AP +1.21 mm versus +0.85 mm; $^{##}p < 0.01$ for AP +0.25 mm versus
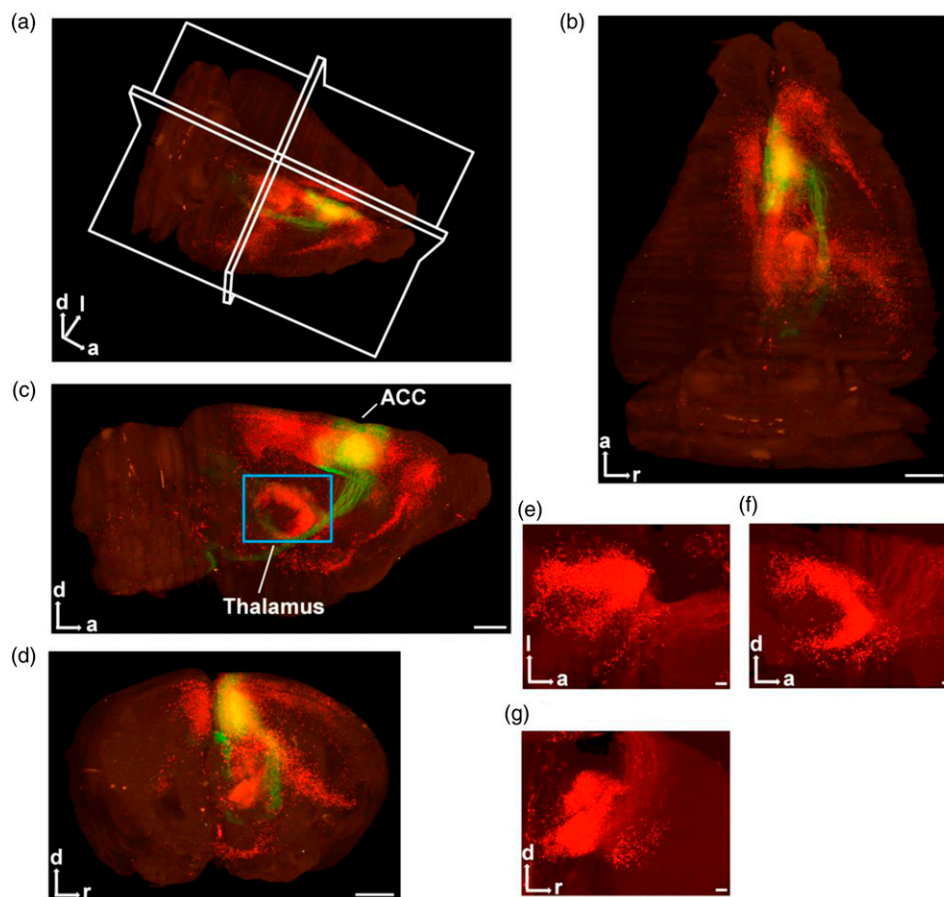
Figure 2. VISoR imaging for rabies virus-injected into the unilateral ACC in adult mouse. **(a)** 3D-reconstructed whole brain in adult mouse. **(b–d)** The horizontal **(b)**, sagittal **(c)** and coronal **(d)** views for one 3D-reconstructed whole brain (red: DsRed$^+$; green: EGFP$^+$). The blue rectangle in **(c)** represents the thalamus. Scale bar: 1 mm. **(e–g)** The horizontal **(e)**, sagittal **(f)** and coronal **(g)** views for the thalamus. Scale bar: 200 μm. a: anterior; d: dorsal; l: left; r: right.

+0.85 mm; unpaired t-test; n = 12 slices/4 mice). Meanwhile, we also found that the ratio of starter to EGFP$^+$ neurons at AP +0.85 mm of the ACC was higher than other coronal sections (Figure 4(e); ratio: 23.11 ± 3.88% at AP +1.21 mm; 34.59 ± 2.53% at AP +0.85 mm; 22.72 ± 1.83% at AP +0.25 mm; $*p <$ 0.05 for AP +1.21 mm versus +0.85 mm; $^{\#\#}p < 0.01$ for AP +0.25 mm versus +0.85 mm; unpaired t-test; n = 12 slices/4 mice).

The neurons which only showed DsRed$^+$ (red) also form monosynaptic connections between different regions of the ACC (Figure 4(c) and (f); cell densities: 712.27 ± 91.01 cells/mm^2 at AP +1.21 mm; 975.19 ± 62.19 cells/mm^2 at AP +0.85 mm; 831.10 ± 53.53 cells/mm^2 at AP +0.25 mm; n = 12 slices/4 mice), including pyramidal neuron–pyramidal neuron, inhibitory neuron–pyramidal neuron, and inhibitory neuron–inhibitory neuron.[5] In the contralateral ACC, we also observed presynaptic inputs (Figure 4(c) and (f); cell densities: 559.46 ± 65.82 cells/mm^2 at AP +1.21 mm; 745.33 ± 56.55 cells/mm^2 at AP +0.85 mm; 623.10 ± 51.67 cells/mm^2 at AP +0.25 mm; n = 12 slices/4 mice), indicating that these

inputs from contralateral ACC send some efferents to the ipsilateral starter neurons.

A typical example of thalamic-anterior cingulate monosynaptic inputs

As described previously, the thalamocortical pathways have complex functions, including sensory perception, motor coordination, and emotion.[4] The connection between thalamus and cortex has attracted more attention. Here, we explored different thalamic nuclei which can send direct projections to the ACC. Four representative slices at different coronal sections were shown in Figure 5(a)–(d). And four different coronal slices contain different thalamic nuclei separately (Figure 5). We found that retrograde labeled neurons to the ACC from the thalamus were predominantly ipsilateral.[18] We also observed that these input neurons to the ACC are mainly distributed in the AM of anterior thalamic nuclei in these two coronal slices (Figure 5(a) and (b); AP −0.83 and −1.07 mm); Except for the AM, the VM, and VAL
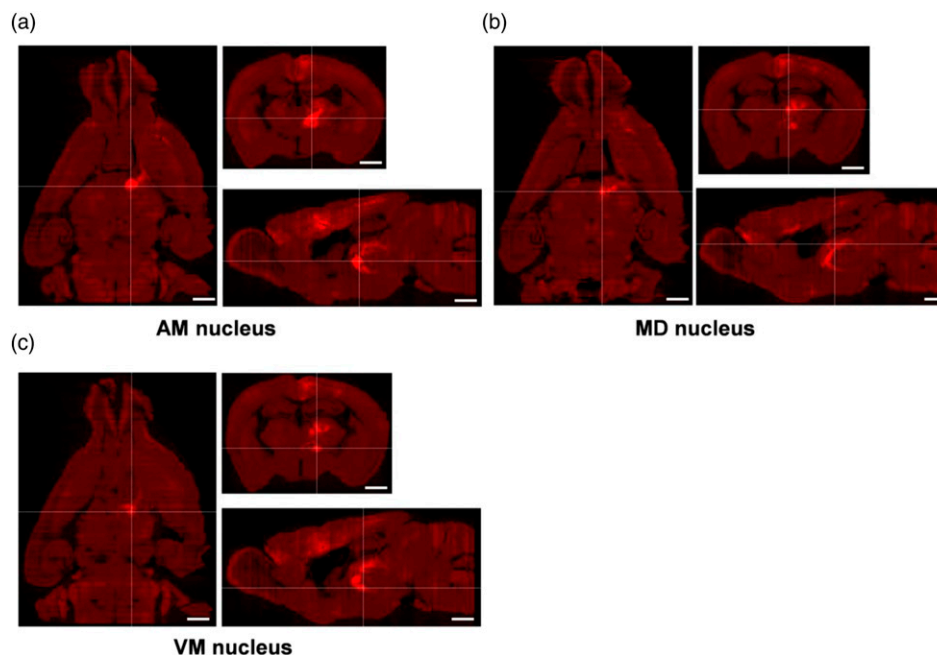
Figure 3. Different sections of the thalamus on one 3D-reconstructed whole brain. **(a–c)** The horizontal, coronal, and sagittal sections are shown according to the intersection of two white lines. The thalamic nuclei at the intersection of two white lines are the AM **(a)**, MD **(b)**, and VM **(c)**, respectively. Scale bar: 1 mm.

of ventral thalamic nuclei send direct projections in the coronal slice located in the AP -1.07 mm (Figure 5(b)); The MDl of medial thalamic nuclei, the CL of intralaminar thalamic nuclei and the lateral thalamic nuclei have also been observed in this coronal slice (AP -1.55 mm) which send major inputs to the ACC (Figure 5(c)). Meanwhile, some other thalamic nuclei that existed in different coronal slices were also observed to send minor projections toward the ACC.

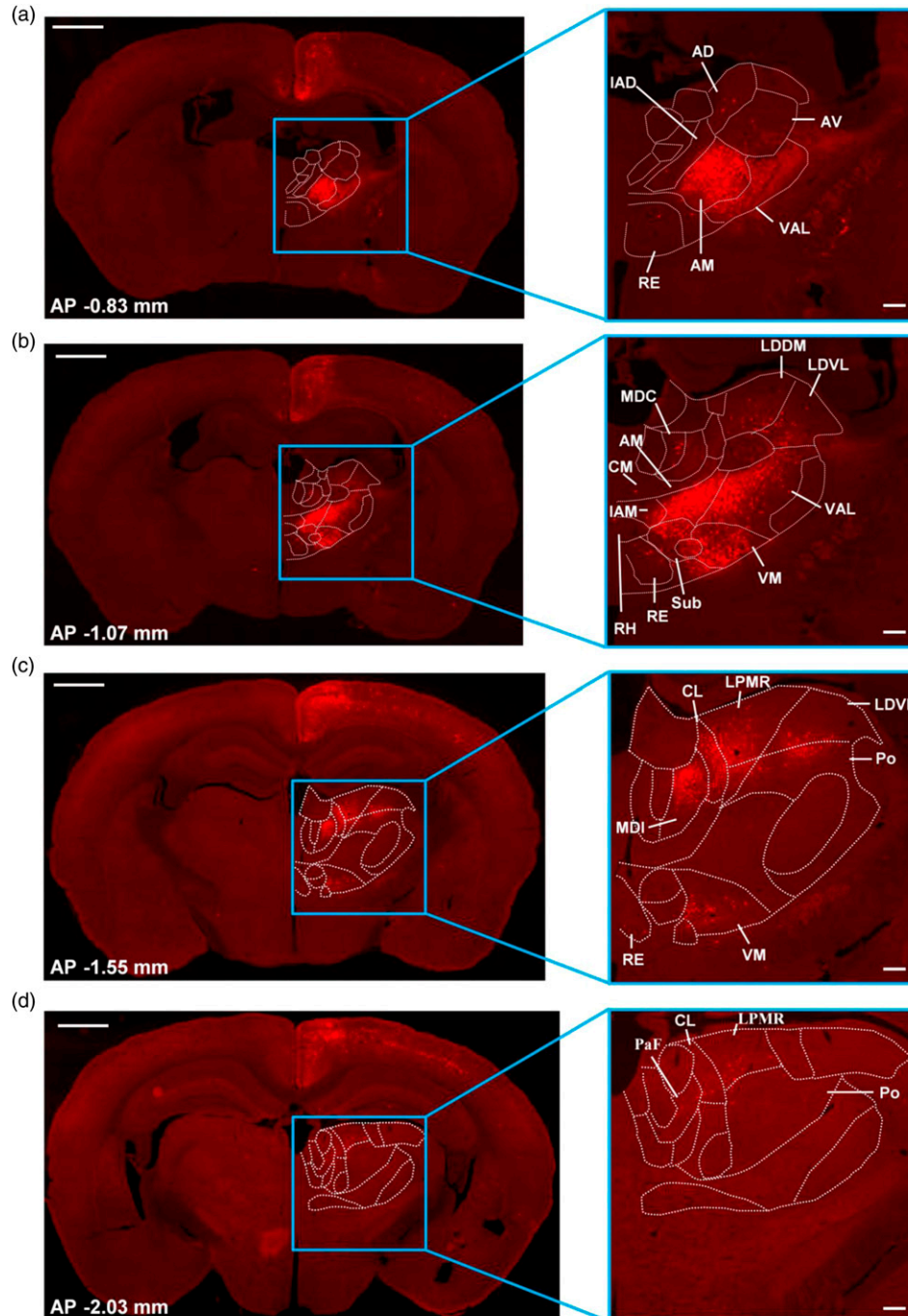## Different thalamic-anterior cingulate monosynaptic inputs from four mice

To observe thalamic-anterior cingulate monosynaptic inputs more clearly, viral micro-injection into unilateral ACC was performed as described above in four mice. Four representative slices of every mouse were selected out and the number of DsRed$^+$ neurons was counted from different thalamic nuclei. And then, we plotted four-slice overlay figures and the histograms at different coronal sections according to the number of DsRed$^+$ neurons in different thalamic nuclei from four mice (Figure 6(a)–(d); mouse 1: red; mouse 2: blue; mouse 3: green; mouse 4: brown). We found that in the coronal slices located in AP −0.83 mm, the AM thalamic nucleus had strong labeling in every mouse; and DsRed$^+$ neurons were also expressed in the VAL, AD, and AV thalamic nuclei of all four coronal slices from four mice (Figure 6(a)). In these coronal slices (AP −1.07 mm), the VAL, AM, VM, MDl, LDDM, LDVL, Sub, and IAM thalamic nuclei contained input neurons to the ACC in all four slices from

four mice. Among them, the ventral and anterior thalamic nuclei contained most of input neurons (Figure 6(b)). The LPMR, MDl, CL, Po, VM, LDVL, and Sub thalamic nuclei had DsRed$^+$ neuronal labeling in all of those coronal slices (AP −1.55 mm), however, these thalamic nuclei from mouse 2 had the relatively small number of input neurons (Figure 6(c)). Meanwhile, four coronal slices located in the AP −2.03 mm contained presynaptic input neurons to the ACC in the PaF and the LPMR thalamic nuclei (Figure 6(d)). In addition, we also observed that DsRed$^+$ neurons from some thalamic nuclei were only expressed in certain mice, but not every mouse. For example, the interanterodorsal thalamic nucleus (IAD), MDl, LDVL, RE, and CM thalamic nuclei in those coronal slices (AP −0.83 mm) had DsRed$^+$ neuronal labeling in certain mice, but not all experimental mice, which may be related with injection site, virus infusion, and expression (Figure 6(a)).

To further understand thalamic-anterior cingulate projections, we also made statistical analysis on the number of DsRed$^+$ neurons (Figure 7(a)), cell densities (Figure 7(b)), and the proportion of input neurons to starter neurons (Figure 7(c)). Those thalamic nuclei were divided into three different types according to the average number of labeled neurons (Strong: $n \geq 20$ neurons; moderate: $10 \leq n < 20$ neurons; light: $n < 10$ neurons). We found that the AM, a major nucleus from anterior thalamic nuclei, projected directly to ipsilateral ACC and showed a dense labeling. In the anterior nuclei, the IAM and AD were also moderately labeled while the IAD and AV were lightly labeled. The mediodorsal nuclei displayed strong
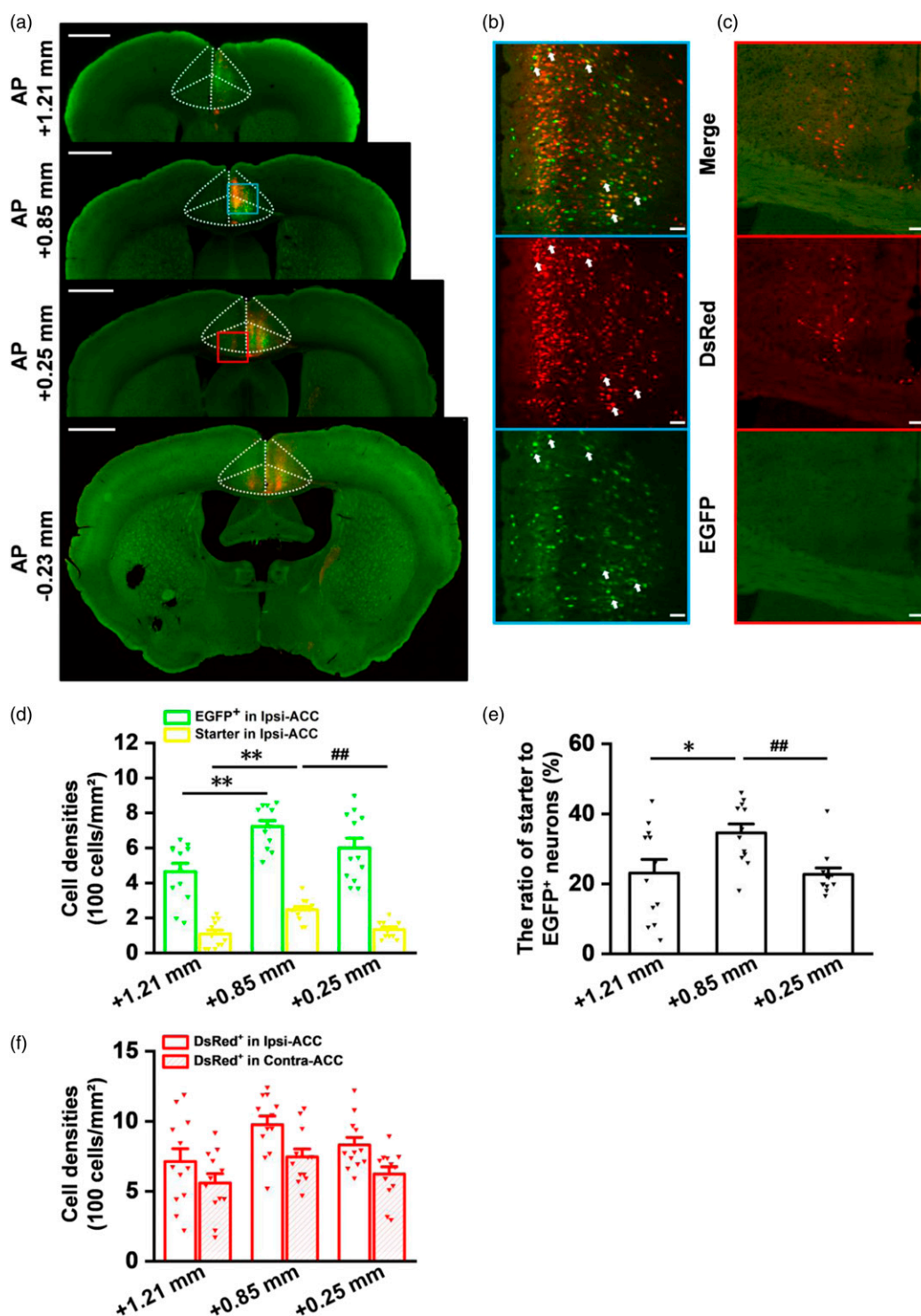
Figure 4. The in-situ viral expression in the injection site of ACC. **(a)** Four different coronal slices (bregma: AP +1.21 mm, +0.85 mm, +0.25 mm, −0.23 mm) show that the helper virus and the rabies virus are both micro-injected into the right ACC (blue rectangle). The white dashed lines represent the anatomic location of the ACC. The red rectangle (DsRed^{+} neurons) represents presynaptic inputs in the left ACC that send direct projections to the starter neurons of the right ACC. Scale bar: 1 mm. **(b)** The enlarged views of the blue-boxed regions in **(a)**. The white arrows indicate infected neurons. Scale bar: 50 μm. **(c)** The enlarged views of the red-boxed regions in **(a)**. **(d)** Cell densities analysis of EGFP^{+} neurons and starter neurons at different coronal sections of the ACC (**$p < 0.01$ for AP +1.21 mm versus +0.85 mm; ##$p < 0.01$ for AP +0.25 mm versus +0.85 mm; unpaired t-test; 3 slices for every mouse; $n = 12$ slices/4 mice). **(e)** Comparisons of the ratio of starter to EGFP^{+} neurons at different coronal sections of the ACC (*$p < 0.05$ for AP +1.21 mm versus +0.85 mm; ##$p < 0.01$ for AP +0.25 mm versus +0.85 mm; unpaired t-test; $n = 12$ slices/4 mice). **(f)** Cell densities analysis of presynaptic inputs at different coronal sections of ipsi- and contra-ACC. $n = 12$ slices/4 mice. The approximate AP level from bregma is indicated. Error bars indicated SEM.
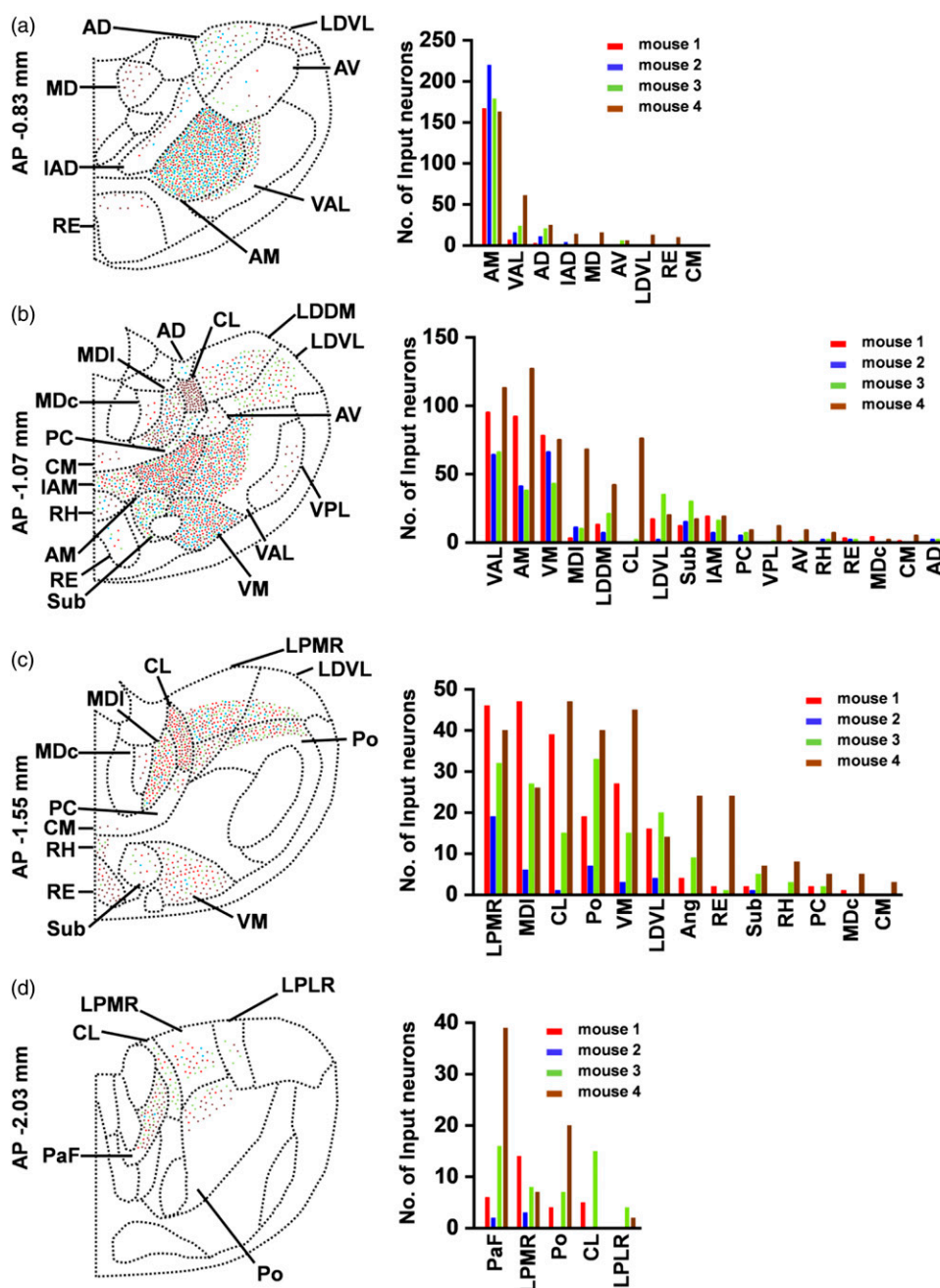
Figure 5. Thalamic-anterior cingulate presynaptic inputs in one typical sample. **(a–d)** Four representative slices are chosen from different coronal slices (bregma: AP −0.83 mm, −1.07 mm, −1.55 mm, −2.03 mm) that contain different thalamic nuclei. These thalamic nuclei contain DsRed$^+$ neurons and their cell densities are different. The enlarged views of the blue rectangle are shown in the right side. Left: scale bar: 1 mm; Right: scale bar: 200 μm. The white dashed lines are drawn according to the Mouse Brain in Stereotaxic Coordinates, 4nd edition, indicating different thalamic nuclei. The approximate AP level from bregma is indicated.

labeling of DsRed$^+$ neurons, especially in the MDl. A light density of retrogradely labeled neurons was observed in the the central part of the mediodorsal thalamic nucleus (MDc). In the ventral group, dense labeling was observed in the VM and VAL nucleus, but light in the ventral posterolateral

thalamic nucleus (VPL). Among the lateral thalamic nuclei, DsRed$^+$ neurons were observed mainly in the LPMR and LDDM; the LDVL sent moderate projections to the ACC, while a light labeling was observed in the laterorostral part of the lateral posterior thalamic nucleus (LPLR). In addition, the
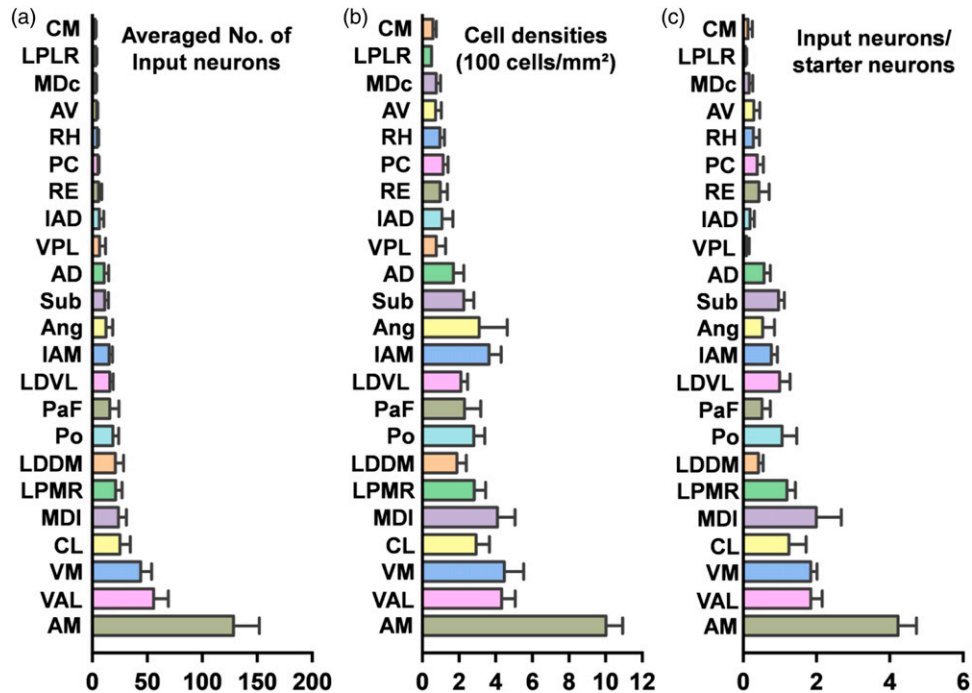
Figure 6. Summary of thalamic-anterior cingulate presynaptic inputs from four adult mice. (**a–d) Left**: Four-slice overlay figures from four mice at different coronal sections (bregma: AP −0.83 mm, −1.07 mm, −1.55 mm, −2.03 mm). The number of DsRed⁺ neurons from different thalamic nuclei of every slice are counted and labeled in schematic graphs according to different coronal sections. **Right**: The histograms of the number of labeled neurons from four mice at different coronal sections (bregma: AP −0.83 mm, −1.07 mm, −1.55 mm, −2.03 mm). The approximate AP level from bregma is indicated. The red, blue, green, and brown dots (left) or columns (right) represent four sequence numbers from mouse 1 to mouse 4 separately.

Po, Ang, and Sub were also labeled moderately. Also, the RE of the midline group contained DsRed⁺ neurons, with light projections to the ACC. Finally, among the intralaminar group, the CL had heavy labeling while the PaF was moderately labeled. We also found that the PC, RH, and CM sent light projections to the ACC.

the ACC. These results show that the thalamus send widespread monosynaptic projections to the ACC and different thalamic nuclei have different input proportions toward the ACC. This tracing technique provides an effective strategy for further explorations of neuronal circuitry and their related functions.

Figure 7. Statistical analysis of thalamic-anterior cingulate presynaptic inputs in adult mice. **(a)** Averaged number of input neurons in different thalamic nuclei. **(b)** Cell densities of input neurons in different thalamic nuclei. **(c)** Ratio of input neurons in different thalamic nuclei to starter neurons in the ACC. *n* = 4 mice. Error bars indicated SEM.

Discussion

The ACC plays vital roles in pain perception and emotions.[5–7] The thalamus is viewed as a relay station that transfers peripheral sensory and motor information to the ACC through thalamocortical pathway.[4] In present study, we utilized the VISoR system to observe 3D-reconstructed whole brain and the thalamus, which can achieve a high-speed, high-throughput, and high-quality brain mapping. Our results show that the ACC neurons receive direct inputs from different thalamic nuclei, including the AM, VM, VAL, CL, MDl, LPMR, LDDM, Po, PaF, LDVL, IAM, Ang, Sub, AD, and other thalamic sub-nuclei that project to the ACC sparsely. Our present results establish the foundation for further study of brain circuitry mechanisms and their related functions.

The advantages of rabies viral tracing strategy and VISoR imaging

Compared with conventional tracing strategies, rabies viral tracing system achieves monosynaptic labeling retrogradely through the manipulation of RVG protein, and presynaptic neurons can be clearly labeled. Furthermore, combined with cre-dependent recombination techniques, this tracing system can target to label defined neuronal subtypes.[22,24,25] The VISoR imaging is a high-throughput technique for whole-brain mapping and is beneficial for long-range tracing of

sparse axons.[19,20] And this approach is compatible with histological labeling, especially immunofluorescence labeling for neuronal specific brain mapping. In the future, this strategy can achieve high-efficiency labeling from other biological samples, even the whole body of different species.[20] In our present study, we ultilized rabies virus-based monosynaptic retrograde tracing system and VISoR imaging for a 3D whole-brain reconstruction to map thalamic-anterior cingulate monosynaptic inputs. Combined with viral tracing techniques, the VISoR imaging has the potential to make us better understand whole-brain anatomic connections and provides systematic insights toward circuitry mechanisms and brain functions.

Functional characteristics of inputs from the thalamus to the ACC

Many studies have shown that different thalamic nuclei send direct projections to the ACC and they play crucial roles in brain functions and behavioral changes. Electrical stimulation of the anterior thalamic nuclei produces plastic changes in the ACC, including paired-pulse facilitation, long-term potentiation and short-term depression, and the anterior thalamic nuclei are involved in spatial navigation and multiple spatial learning tasks.[26,27] Our results show that DsRed⁺ neurons are observed in the AM, IAM, AD, IAD, and AV of the anterior thalamic nuclei. And different anterior thalamic nuclei are responsible for different aspects of spatial processing, such as

direction, place, and temporal information.[26] Consistent with our results, previous studies have shown that AM send direct projections to corticotropin-releasing hormone (CRH), GABAergic, and glutamatergic neurons of the ACC.[18,22,25] The pathway from the AM thalamic nucleus to the ACC has been shown to modulate histaminergic itch-induced scratching behaviors.[28] The AM thalamic nucleus is also involved in social defeat-associated contextual fear memory.[29] Different with previous study in rats,[15] we find that the AD and AV send moderate projections to the ACC in adult mice.[30] Some reports have shown that the AD send direct projections to area 24a, but not 24b in adult mice.[18] However, we haven't differentiated 24a and 24b. Overall, these anatomical connections may provide new perspectives for further study of anterior thalamic-ACC circuitry mechanisms.

As previously described, our results also show that MD, especially the MDl nucleus, send a dense projection to the ACC, which is involved in nociceptive processing.[31] Experimental activation of MD neurons leads to enhanced nociceptive-like activities in the ACC.[9,32] Pain experience may also remodel the MD-ACC projection to modify nociceptive sensitivity.[33] Chronic pain alters the balance between excitation and feed-forward inhibition from MD-ACC input to shift toward inhibition, which in turn promotes pain-related aversion.[34] Studies also have shown that the MD neurons directly excite parvalbumin-positive interneurons in the dorsal ACC to mediate feed-forward inhibition of layer III of the ACC, which is thought to be involved in cognitive regulation.[35] These results provide a therapeutic strategy for nociceptive processing and some cognitive diseases.

In addition to the anterior and medial nuclei, the VM and VAL of the ventral thalamic nuclei also provide dense inputs to the ACC. The ventral thalamic nuclei play important roles in motor control[36] and the VM neurons are clearly activated by both Aδ- and C-fibers to transmit nociceptive signals to the frontal cortex.[37,38] Therefore, the ventral thalamic nuclei are responsible for escape from nociceptive stimulus.[18] In the lateral group of thalamus, the laterodorsal (LD) and lateral posterior (LP) thalamic nuclei, which are helpful for visual processing, spatial orientation, and learning tasks,[39,40] also project directly to the ACC. The projection from the LP to the ACC also plays important roles in directed attention and contralateral neglect.[41] Furthermore, the projection from posterior thalamic nucleus to the ACC is thought to be associated with migraine-related affective/motivational behaviors.[42] In the intralaminar and midline group, the ACC directly receives some projections from the PaF, CL, PC, RH, CM, and RE nuclei, which are involved in specific cognitive, sensory, and motor functions.[43] Among them, the PaF-ACC pathway takes part into the regulation of depression-like pain.[18,25]

Overall, our results provide exact evidence toward thalamic-anterior cingulate monosynaptic inputs. And some studies have reported these direct inputs are involved in pain, learning memory, motor control, cognitive regulation and so on. These fundamental anatomic evidences would be helpful for future functional studies and treatment of neurological diseases.

Authors' contributions

M.X., F.X., G.Q.B., X.H.L., J.S.L. and M.Z. designed the experiments. M.X., W.T.S., S.B.Z., Y.N.L., F.Y.W., Q.Y.C., R.H.L., Z.X.Z., Y.X.Z. and Y.X.C. performed experiments and analyzed data. M.X., Q.Y.C., X.H.L., J.S.L., and M.Z. drafted the manuscript and finished the final version of the manuscript. All authors read and approved the final manuscript.

Declaration of conflicting interests

The author(s) declared no potential conflicts of interest with respect to the research, authorship, and/or publication of this article.

ORCID iDs

Qi-Yu Chen ⓘ https://orcid.org/0000-0002-5707-6220
Xu-Hui Li ⓘ https://orcid.org/0000-0003-4376-6252
Jing-Shan Lu ⓘ https://orcid.org/0000-0002-7330-6567

References

1. Bordes S, Werner C, Mathkour M, McCormack E, Iwanaga J, Loukas M, Lammle M, Dumont AS, Tubbs RS. Arterial supply of the Thalamus: a comprehensive review. *World Neurosurg* 2020; 137: 310–318. DOI: 10.1016/j.wneu.2020.01.237.

2. Sherman SM. Functioning of circuits connecting Thalamus and cortex. *Compr Physiol* 2017; 7: 713–739. DOI: 10.1002/cphy.c160032.

3. Oh SW, Harris JA, Ng L, Winslow B, Cain N, Mihalas S, Wang Q, Lau C, Kuan L, Henry AM, Mortrud MT, Ouellette B, Nguyen TN, Sorensen SA, Slaughterbeck CR, Wakeman W, Li Y, Feng D, Ho A, Nicholas E, Hirokawa KE, Bohn P, Joines KM, Peng H, Hawrylycz MJ, Phillips JW, Hohmann JG, Wohnoutka P, Gerfen CR, Koch C, Bernard A, Dang C, Jones AR, Zeng H. A mesoscale connectome of the mouse brain. *Nature* 2014; 508: 207–214. DOI: 10.1038/nature13186.

4. Brandt T, Dieterich M. Thalamocortical network: a core structure for integrative multimodal vestibular functions. *Curr Opin Neurol* 2019; 32: 154–164. DOI: 10.1097/WCO.0000000000000638.

5. Bliss TV, Collingridge GL, Kaang BK, Zhuo M. Synaptic plasticity in the anterior cingulate cortex in acute and chronic pain. *Nat Rev Neurosci* 2016; 17: 485–496. DOI: 10.1038/nrn.2016.68.

6. Zhuo M. Cortical excitation and chronic pain. *Trends Neurosci* 2008; 31: 199–207. DOI: 10.1016/j.tins.2008.01.003.

7. Zhuo M. Neural mechanisms underlying anxiety-chronic pain interactions. *Trends Neurosci* 2016; 39: 136–145. DOI: 10.1016/j.tins.2016.01.006.

8. Kung JC, Shyu BC. Potentiation of local field potentials in the anterior cingulate cortex evoked by the stimulation of the medial thalamic nuclei in rats. *Brain Res* 2002; 953: 37–44. DOI: 10.1016/s0006-8993(02)03265-1.

9. Shyu BC, Vogt BA. Short-term synaptic plasticity in the nociceptive thalamic-anterior cingulate pathway. *Mol Pain* 2009; 5: 51. DOI: 10.1186/1744-8069-5-51.

10. Vogt LJ, Vogt BA, Sikes RW. Limbic thalamus in rabbit: architecture, projections to cingulate cortex and distribution of muscarinic acetylcholine, GABAA, and opioid receptors. *J Comp Neurol* 1992; 319: 205–217. DOI: 10.1002/cne.903190203.

11. Jurgens U. Afferent fibers to the cingular vocalization region in the squirrel monkey. *Exp Neurol* 1983; 80: 395–409. DOI: 10.1016/0014-4886(83)90291-1.

12. Vogt BA, Pandya DN, Rosene DL. Cingulate cortex of the rhesus monkey: I. Cytoarchitecture and thalamic afferents. *J Comp Neurol* 1987; 262: 256–270. DOI: 10.1002/cne.902620207.

13. Thompson SM, Robertson RT. Organization of subcortical pathways for sensory projections to the limbic cortex. I. Subcortical projections to the medial limbic cortex in the rat. *J Comp Neurol* 1987; 265: 175–188. DOI: 10.1002/cne.902650203.

14. Conde F, Maire-Lepoivre E, Audinat E, Crepel F. Afferent connections of the medial frontal cortex of the rat. II. Cortical and subcortical afferents. *J Comp Neurol* 1995; 352: 567–593. DOI: 10.1002/cne.903520407.

15. Hoover WB, Vertes RP. Anatomical analysis of afferent projections to the medial prefrontal cortex in the rat. *Brain Struct Funct* 2007; 212: 149–179. DOI: 10.1007/s00429-007-0150-4.

16. Robertson RT, Kaitz SS. Thalamic connections with limbic cortex. I. Thalamocortical projections. *J Comp Neurol* 1981; 195: 501–525. DOI: 10.1002/cne.901950308.

17. Musil SY, Olson CR. Organization of cortical and subcortical projections to anterior cingulate cortex in the cat. *J Comp Neurol* 1988; 272: 203–218. DOI: 10.1002/cne.902720205.

18. Fillinger C, Yalcin I, Barrot M, Veinante P. Afferents to anterior cingulate areas 24a and 24b and midcingulate areas 24a' and 24b' in the mouse. *Brain Struct Funct* 2017; 222: 1509–1532. DOI: 10.1007/s00429-016-1290-1.

19. Wang H, Zhu QY, Ding LF, Shen Y, Yang CY, Xu F, Shu C, Guo YJ, Xiong ZW, Shan QH, Jia F, Su P, Yang QR, Li B, Cheng YX, He XB, Chen X, Wu F, Zhou JN, Xu FQ, Han H, Lau PM, Bi GQ. Scalable volumetric imaging for ultrahigh-speed brain mapping at synaptic resolution. *Natl Sci Rev* 2019; 6: 982–992. DOI: 10.1093/nsr/nwz053.

20. Xu F, Shen Y, Ding L, Yang CY, Tan H, Wang H, Zhu Q, Xu R, Wu F, Xiao Y, Xu C, Li Q, Su P, Zhang LI, Dong HW, Desimone R, Xu F, Hu X, Lau PM, Bi GQ. High-throughput mapping of a whole rhesus monkey brain at micrometer resolution. *Nat Biotechnol* 2021. DOI: 10.1038/s41587-021-00986-5.

21. Chen T, Koga K, Descalzi G, Qiu S, Wang J, Zhang LS, Zhang ZJ, He XB, Qin X, Xu FQ, Hu J, Wei F, Huganir RL, Li YQ, Zhuo M. Postsynaptic potentiation of corticospinal projecting neurons in the anterior cingulate cortex after nerve injury. *Mol Pain* 2014; 10: 33. DOI: 10.1186/1744-8069-10-33.

22. Zhang S, Lv F, Yuan Y, Fan C, Li J, Sun W, Hu J. Whole-brain mapping of monosynaptic afferent inputs to cortical CRH Neurons. *Front Neurosci* 2019; 13: 565. DOI: 10.3389/fnins.2019.00565.

23. Berendse HW, Groenewegen HJ. Restricted cortical termination fields of the midline and intralaminar thalamic nuclei in the rat. *Neuroscience* 1991; 42: 73–102. DOI: 10.1016/0306-4522(91)90151-d.

24. Zhang S, Xu M, Chang WC, Ma C, Hoang Do JP, Jeong D, Lei T, Fan JL, Dan Y. Organization of long-range inputs and outputs of frontal cortex for top-down control. *Nat Neurosci* 2016; 19: 1733–1742. DOI: 10.1038/nn.4417.

25. Zhu X, Tang HD, Dong WY, Kang F, Liu A, Mao Y, Xie W, Zhang X, Cao P, Zhou W, Wang H, Farzinpour Z, Tao W, Song X, Zhang Y, Xue T, Jin Y, Li J, Zhang Z. Distinct thalamocortical circuits underlie allodynia induced by tissue injury and by depression-like states. *Nat Neurosci* 2021; 24: 542–553. DOI: 10.1038/s41593-021-00811-x.

26. Aggleton JP, Nelson AJ. Why do lesions in the rodent anterior thalamic nuclei cause such severe spatial deficits? *Neurosci Biobehav Rev* 2015; 54: 131–144. DOI: 10.1016/j.neubiorev.2014.08.013.

27. Gemmell C, O'Mara SM. Plasticity in the projection from the anterior thalamic nuclei to the anterior cingulate cortex in the rat in vivo: paired-pulse facilitation, long-term potentiation and short-term depression. *Neuroscience* 2002; 109: 401–406. DOI: 10.1016/s0306-4522(01)00554-1.

28. Deng YZ, Lu YC, Wu WW, Cheng L, Zan GY, Chai JR, Wang YJ, Chen Z, Liu JG. Anteromedial thalamic nucleus to anterior cingulate cortex inputs modulate histaminergic itch sensation. *Neuropharmacology* 2020; 168: 108028. DOI: 10.1016/j.neuropharm.2020.108028.

29. Rangel MJ Jr, Baldo MVC, Canteras NS. Influence of the anteromedial thalamus on social defeat-associated contextual fear memory. *Behav Brain Res* 2018; 339: 269–277. DOI: 10.1016/j.bbr.2017.10.038.

30. Horikawa K, Kinjo N, Stanley LC, Powell EW. Topographic organization and collateralization of the projections of the anterior and laterodorsal thalamic nuclei to cingulate areas 24 and 29 in the rat. *Neurosci Res* 1988; 6: 31–44. DOI: 10.1016/0168-0102(88)90004-1.

31. Yen CT, Lu PL. Thalamus and pain. *Acta Anaesthesiol Taiwan* 2013; 51: 73–80. DOI: 10.1016/j.aat.2013.06.011.

32. Sun JJ, Chuang Kung J, Wang CC, Chen SL, Shyu BC. Short-term facilitation in the anterior cingulate cortex following stimulation of the medial thalamus in the rat. *Brain Res* 2006; 1097: 101–115. DOI: 10.1016/j.brainres.2006.04.065.

33. Wang YQ, Wang J, Xia SH, Gutstein HB, Huang YH, Schluter OM, Cao JL, Dong Y. Neuropathic pain generates silent synapses in thalamic projection to anterior cingulate cortex. *Pain* 2021; 162: 1322–1333. DOI: 10.1097/j.pain. 0000000000002149.

34. Meda KS, Patel T, Braz JM, Malik R, Turner ML, Seifikar H, Basbaum AI, Sohal VS. Microcircuit mechanisms through which mediodorsal thalamic input to anterior cingulate cortex exacerbates pain-related aversion. *Neuron* 2019; 102: 944–959.e943. DOI: 10.1016/j.neuron.2019.03.042.

35. Delevich K, Tucciarone J, Huang ZJ, Li B. The mediodorsal thalamus drives feedforward inhibition in the anterior cingulate cortex via parvalbumin interneurons. *J Neurosci* 2015; 35: 5743–5753. DOI: 10.1523/JNEUROSCI.4565-14.2015.

36. Klockgether T, Schwarz M, Turski L, Sontag KH. The rat ventromedial thalamic nucleus and motor control: role of N-methyl-D-aspartate-mediated excitation, GABAergic inhibition, and muscarinic transmission. *J Neurosci* 1986; 6: 1702–1711.

37. Monconduit L, Bourgeais L, Bernard JF, Le Bars D, Villanueva L. Ventromedial thalamic neurons convey nociceptive signals from the whole body surface to the dorsolateral neocortex. *J Neurosci* 1999; 19: 9063–9072.

38. Monconduit L, Villanueva L. The lateral ventromedial thalamic nucleus spreads nociceptive signals from the whole body surface to layer I of the frontal cortex. *Eur J Neurosci* 2005; 21: 3395–3402. DOI: 10.1111/j.1460-9568.2005.04160.x.

39. Bezdudnaya T, Keller A. Laterodorsal nucleus of the thalamus: a processor of somatosensory inputs. *J Comp Neurol* 2008; 507: 1979–1989. DOI: 10.1002/cne.21664.

40. Allen AE, Procyk CA, Howarth M, Walmsley L, Brown TM. Visual input to the mouse lateral posterior and posterior thalamic nuclei: photoreceptive origins and retinotopic order. *J Physiol* 2016; 594: 1911–1929. DOI: 10.1113/JP271707.

41. Conte WL, Kamishina H, Corwin JV, Reep RL. Topography in the projections of lateral posterior thalamus with cingulate and medial agranular cortex in relation to circuitry for directed attention and neglect. *Brain Res* 2008; 1240: 87–95. DOI: 10. 1016/j.brainres.2008.09.013.

42. Brennan KC, Pietrobon D. A systems neuroscience approach to migraine. *Neuron* 2018; 97: 1004–1021. DOI: 10.1016/j. neuron.2018.01.029.

43. Van der Werf YD, Witter MP, Groenewegen HJ. The intralaminar and midline nuclei of the thalamus. Anatomical and functional evidence for participation in processes of arousal and awareness. *Brain Res Brain Res Rev* 2002; 39: 107–140. DOI: 10.1016/s0165-0173(02)00181-9.

44. Finch DM, Derian EL, Babb TL. Afferent fibers to rat cingulate cortex. *Exp Neurol* 1984; 83: 468–485. DOI: 10.1016/0014-4886(84)90116-x.

45. Conde F, Audinat E, Maire-Lepoivre E, Crepel F. Afferent connections of the medial frontal cortex of the rat. A study using retrograde transport of fluorescent dyes. I. Thalamic afferents. *Brain Res Bull* 1990; 24: 341–354. DOI: 10.1016/0361-9230(90)90088-h.

46. Vogt BA, Rosene DL, Pandya DN. Thalamic and cortical afferents differentiate anterior from posterior cingulate cortex in the monkey. *Science* 1979; 204: 205–207. DOI: 10.1126/science.107587.

47. Baleydier C, Mauguiere F. The duality of the cingulate gyrus in monkey. Neuroanatomical study and functional hypothesis. *Brain* 1980; 103: 525–554. DOI: 10.1093/brain/103.3.525.

48. Macchi G, Bentivoglio M, Molinari M, Minciacchi D. The thalamo-caudate versus thalamo-cortical projections as studied in the cat with fluorescent retrograde double labeling. *Exp Brain Res* 1984; 54: 225–239. DOI: 10.1007/BF00236222.

49. Cruikshank SJ, Ahmed OJ, Stevens TR, Patrick SL, Gonzalez AN, Elmaleh M, Connors BW. Thalamic control of layer 1 circuits in prefrontal cortex. *J Neurosci* 2012; 32: 17813–17823. DOI: 10.1523/JNEUROSCI.3231-12.2012.